Therapeutics, Targets, and Chemical Biology

Cancer Research

Targeting Protein Synthesis in a Myc/mTOR-Driven Model of Anorexia-Cachexia Syndrome Delays Its Onset and Prolongs Survival

Francis Robert[1], John R. Mills[1], Aouod Agenor[1], Dantong Wang[2], Sergio DiMarco[1], Regina Cencic[1], Michel L. Tremblay[1,3,6], Imed Eddine Gallouzi[1,6], Siegfried Hekimi[2], Simon S. Wing[1,4,7], and Jerry Pelletier[1,3,6]

Abstract

Anorexia-cachexia syndrome (ACS) is a major determinant of cancer-related death that causes progressive body weight loss due to depletion of skeletal muscle mass and body fat. Here, we report the development of a novel preclinical murine model of ACS in which lymphomas harbor elevated Myc and activated mTOR signaling. The ACS phenotype in this model correlated with deregulated expression of a number of cytokines, including elevated levels of interleukin-10 which was under the direct translational control of mTOR. Notably, pharmacologic intervention to impair protein synthesis restored cytokine production to near-normal levels, delayed ACS progression, and extended host survival. Together, our findings suggest a new paradigm to treat ACS by strategies which target protein synthesis to block the production of procachexic factors. *Cancer Res; 72(3); 747–56. ©2011 AACR.*

Introduction

Anorexia-cachexia syndrome (ACS) is characterized by loss of adipose tissue and skeletal muscle mass that leads to weight loss exceeding 10% of the patient's preillness weight (1, 2). ACS affects 80% of advanced patients with cancer and impacts on the survival of patients, response to chemotherapy, and overall quality of life—accounting for approximately 30% of cancer-related deaths. The underlying mechanisms responsible for ACS remains obscure, but are thought to be multifactorial, resulting from an imbalance of pro- and anti-inflammatory cytokines and orexigenic and anorexigenic factors (1). Altered expression of several cytokines and growth factors (e.g., TNF-α, IL-1, IL-6, IGF-1, and IFN-γ) have been implicated in cancer cachexia (3–8).

The PI3K-Akt-mTOR pathway is one of the most frequently perturbed signaling cascades in human cancers (9) and serves to integrate extra- and intracellular inputs from a large number of sources to fine tune cellular proliferation and growth. One key event downstream of mTOR regulated by this pathway is the ribosome recruitment phase of translation initiation. Ribosome recruitment is mediated by eukaryotic initiation factor (eIF)4F, a complex consisting of eIF4E, the cap (m^7GpppN; where N is any nucleotide) binding protein; eIF4A, an RNA helicase; and eIF4G, a large scaffolding protein (10). mTOR regulates translation initiation rates by controlling the availability of eIF4E and eIF4A for assembly into the eIF4F complex (10). Thus, loss of the tumor suppressors, PTEN, TSC1, or TSC2, lead to activation of the mTOR kinase and elevated translation initiation rates. Small molecules that target mTOR or eIF4F reverse chemoresistance in preclinical cancer models (11, 12).

In the Eμ-Myc lymphoma model, where Myc overexpression is driven by the lymphoid-specific IgH enhancer (Eμ) in the pre-B/B-cell compartment (13), lesions in the Akt-Tsc1/2 pathway accelerate lymphomagenesis (11, 14). Here, we describe a new murine model of ACS consisting of pre-B/B-lymphoma cells overexpressing Myc and exhibiting activated mTOR signaling due to loss of the PTEN, TSC1, or TSC2 tumor suppressor genes. We take advantage of the powerful genetics of this model to develop a new paradigm for treating ACS consisting of targeting protein synthesis to curtail aberrant production of procachexic factors.

Materials and Methods

Mouse studies

$Tsc2^{+/-}$Eμ-Myc, $Tsc1^{+/-}$Eμ-Myc, and $Pten^{+/-}$Eμ-Myc lymphomas were generated from crosses between $Tsc2^{+/-}$, $Tsc1^{+/-}$, and $Pten^{+/-}$ to Eμ-Myc mice. All strains have been inbred on the C57BL/6 (Charles River Laboratories) background for more than 10 generations. In the Eμ-Myc model, disease is characterized by palpable lymph nodes, evidence of circulating leukemic cells, and enlarged spleens (13).

For treatment studies, C57BL/6 males were injected with 2 million $Tsc2^{+/-}$Eμ-Myc/Mcl-1 cells. Rapamycin or

Authors' Affiliations: Departments of [1]Biochemistry, [2]Biology, [3]Oncology, [4]Medicine, and [5]Epidemiology and Biostatistics, [6]The Rosalind and Morris Goodman Cancer Center, and [7]McGill University Health Centre Research Institute, McGill University, Montreal, Quebec, Canada

Note: Supplementary data for this article are available at Cancer Research Online (http://cancerres.aacrjournals.org/).

Corresponding Author: Jerry Pelletier, McIntyre Medical Sciences Building, Rm 810, 3655 Promenade Sir-William-Osler, McGill University, Montreal, Quebec, Canada H3G 1Y6. Phone: 514-398-2323; Fax: 514-398-7384; E-mail: jerry.pelletier@mcgill.ca

doi: 10.1158/0008-5472.CAN-11-2739

homoharringtonine treatments were initiated 3 and 5 days following cell transplant, respectively, and continued every day for the indicated times. A complete remission is defined as the absence of palpable tumor and leukemia. Tumor-free survival is defined as the time between treatment and reappearance of a palpable lymphoma. Overall survival is defined as the time between treatment and progression to a terminal stage at which point the animals were euthanized. The terminal stage is defined by the McGill University Faculty of Medicine Animal Care Committee which uses the body condition score (BCS) method (15). We used a BCS < 2 which includes decreased exploratory behavior, reluctance to move (decreased locomotion/mobility), pronounced hunched posture, piloerection, moderate to severe dehydration (sunken eyes, prolonged skin tent, and lethargy), and unrelenting pain (e.g., distress vocalization). All animal studies were approved by the McGill University Faculty of Medicine Animal Care Committee. Data were analyzed in the Kaplan–Meier format using the log-rank (Mantel–Cox) test for statistical significance.

For the C26 colon cancer cachexia model, a tumor section was obtained from the National Cancer Institute, Bethesda, MD, and surgically transplanted into the flank of a 6 week-old male BALB/c mouse. Two weeks after engraftment, cells were extracted by mincing the tumor in PBS, followed by multiple passages through syringes with decreasing size. Finally, the resulting suspension was trypsinized by incubation with 0.25% trypsin and grown in RPMI-1640 medium. Except for their ability to induce cachexia, no further authentication was carried out on the C26 cell line. For transplantation studies, 2×10^6 cells were resuspended in 100-μL PBS and injected in the right flank of 4- to 6-week-old male BALB/c mice.

Serum harvesting and cytokine profiling

For serum collection, mice were anesthetized with tribromoethanol (240 mg/kg) and blood harvested by heart puncture with a 25 gauge needle and transferred to BD Microtainer serum separator tubes (BD Biosciences). Serum was prepared and cytokine determinations conducted on a Biorad Bio-Plex reader which allows multiple cytokines to be profiled from single samples. Leptin (Assay Design), CRP (Immunology Consultants Laboratory, Inc.), acetylated ghrelin (SPI-Bio), interleukin-10 (IL-10; eBioscience), and neuropeptide Y (NPY; Peninsula Laboratories) levels were determined by ELISA assays conducted according to the manufacturer's recommendations. Serum levels of glucose were determined by the glucose (GO) assay kit (Sigma).

Indirect calorimetric assay

Eight mice were individually subjected to indirect calorimetry (Columbus Instruments). Measurements on $Tsc2^{+/-}$Eμ-Myc and Eμ-Myc tumor-bearing mice were carried out for 2 weeks in a special experimental room with stable room temperature and automatic light control (7–19 hours). Body weight was recorded every day. The concentrations of input and output oxygen and carbon dioxide (CO_2) were detected by built-in oxygen and CO_2 sensors, respectively. The oxygen consumption and CO_2 production were deduced from the difference between input and output values. The total energy expenditure (heat production) and the respiratory exchange ratio (RER) were calculated as described previously (16). Because of changes in body weight, the average weight of 2 consecutive days was used to calculate the per-weight oxygen and CO_2 consumptions.

Real-time quantitative reverse transcription PCR measurements

For monitoring muscle gene expression, RNA was prepared from gastrocnemius muscles by solubilization in guanidium isothiocyanate followed by centrifugation on a CsCl cushion. cDNA was prepared from the RNA using reverse transcriptase and oligo (dT) as primer. Quantitative PCR was conducted on the cDNA samples using primers listed in Supplementary Table S1.

Polysomal RNA isolation and qRT-PCR were carried out as described (14). The primers used for qRT-PCR were: IL-10 forward (336–356), 5′-ACCTGGTAGAAGTGATGCCCC-3′; IL-10 reverse (553–572), 5′-CTATGCAGTTGATGAAGATG-3′; β-actin forward (822–844), 5′-TCACTATTGGCAACGAGCGGTT-3′; and β-actin reverse (1,013–991), 5′-TGTCAGCAATGCCTGGGTACAT-3′.

Results

Mice bearing Eμ-Myc lymphomas harboring loss of the *PTEN* or *TSC1*/2 tumor suppressors develop cardinal features of ACS

During the course of tumor transplantation studies into C57BL/6 mice (Supplementary Fig. S1A), we noted that $Tsc2^{+/-}$Eμ-Myc and $Pten^{+/-}$Eμ-Myc tumor-bearing animals showed significantly reduced survival times compared with mice harboring Eμ-Myc tumors, despite having received the same number of cells during transplant (Fig. 1A). The observed decrease in survival was not due to increased tumor burden as $Tsc2^{+/-}$Eμ-Myc and $Pten^{+/-}$Eμ-Myc tumor-bearing animals presented with smaller inguinal tumors (Supplementary Fig. S1B), equivalent or reduced $B220^+$ tumor cells (Supplementary Fig. S1C), and reduced spleen weights (Supplementary Fig. S1D). Notably, $Tsc2^{+/-}$Eμ-Myc and $Pten^{+/-}$Eμ-Myc tumor-bearing mice showed a rapid and severe loss of body weight starting at 9 and 11 days, respectively, after transplantation (Fig. 1B). This was in contrast to mice bearing Eμ-Myc lymphomas who continued to gain weight over the course of the experiment at a rate comparable with wild-type C57BL/6 mice (Fig. 1B). Mice bearing $Tsc2^{+/-}$Eμ-Myc or $Pten^{+/-}$Eμ-Myc lymphomas also showed complete loss of adipose tissue (which occurred before the experimental endpoint; Fig. 1C) as well as significant loss of muscle mass (Fig. 1D and Supplementary Fig. S1E). To determine the relative rates at which muscle mass and adipose tissue were lost, a cohort of mice were injected with either $Tsc2^{+/-}$Eμ-Myc or Eμ-Myc tumor cells and at specified times, animals were sacrificed and muscle and adipose fat mass was measured. We found that muscle mass and epididymal fat loss occurred concurrently indicating that the reduction in muscle mass was not a secondary consequence due to the absence of adipose tissue (Supplementary Fig. S2). Mice bearing tumor cells in which mTOR signaling was not activated, such as Eμ-Myc or Eμ-Myc/Bcl-2

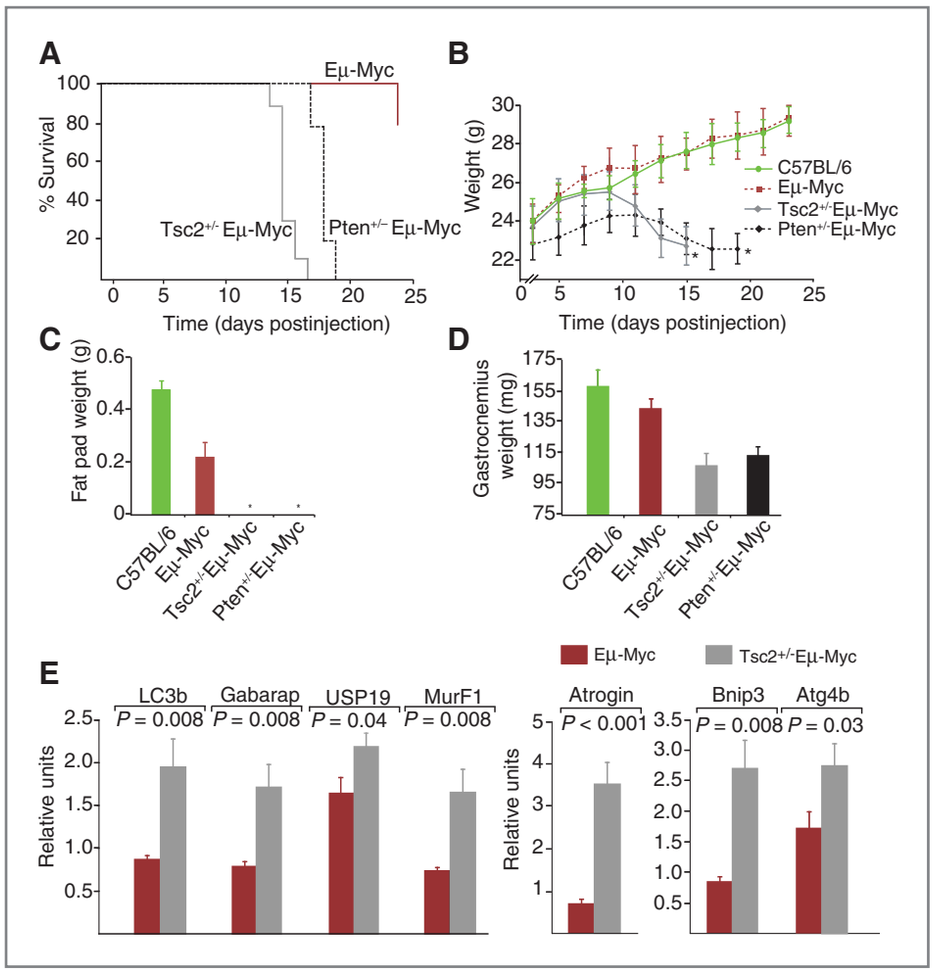

Figure 1. Mice bearing Tsc2$^{+/-}$ Eμ-Myc or Pten$^{+/-}$Eμ-Myc lymphomas display cardinal features of human ACS. A, Kaplan–Meier curve showing survival rate of C57BL/6 mice harboring Eμ-Myc, Pten$^{+/-}$Eμ-Myc, and Tsc2$^{+/-}$ Eμ-Myc lymphomas following adoptive transfer. $n = 10$ mice/cohort; $P < 0.001$ for both Pten$^{+/-}$ Eμ-Myc and Tsc2$^{+/-}$Eμ-Myc relative to Eμ-Myc. B, changes in body weight of C57BL/6 mice harboring tumors of the indicated genotypes. Values are mean ± SEM; $n = 5$ mice. *, indicates termination of experiment due to progression to endpoint. C, epididymal fat pad weights of C57BL/6 mice bearing tumors of the indicated genotypes. Tissues were harvested at the end of the experiment in (B). Values are mean ± SEM; $n = 5$ mice. *, no fat pad remaining. D, weight of gastrocnemius muscle of C57BL/6 mice bearing tumors of the indicated genotypes. Tissues were harvested at the end of the experiment in (B). Values are mean ± SEM; $n = 5$ mice. E, transcript levels for the indicated genes were determined by qRT-PCR from skeletal muscle RNA harvested from C57BL/6 mice bearing Eμ-Myc or Tsc2$^{+/-}$Eμ-Myc lymphomas. Values are normalized to the housekeeping gene, porphobilinogen deaminase (PBGD) and expressed as mean ± SEM; $n = 5$ samples.

lymphomas, did not show this general "wasting" phenotype (Supplementary Fig. S3). The muscle loss observed in Tsc2$^{+/-}$Eμ-Myc tumor-bearing animals was attributable, at least in part, to activation of intracellular proteolysis as reflected by increased expression of key markers of the ubiquitin and autophagic systems (Fig. 1E). This included elevated muscle expression of the ubiquitin protein ligases MuRF1 and MAFbx/atrogin-1 (17, 18), the deubiquitinating enzyme USP19 (19), and the autophagy genes LC3b, Gabarap, Bnip3, and Atg4b (20) in Tsc2$^{+/-}$Eμ-Myc tumor-bearing mice compared with Eμ-Myc tumor-bearing mice (Fig. 1E) and indicate the presence of an active catabolic process in muscle of Tsc2$^{+/-}$Eμ-Myc tumor-bearing mice.

Mice harboring Tsc2$^{+/-}$Eμ-Myc tumors also have reduced appetite compared with those bearing Eμ-Myc tumors (Fig. 2A). To determine whether this reduced caloric intake could account for the reduction in body mass noted among Tsc2$^{+/-}$Eμ-Myc tumor-bearing animals (Fig. 1B), we carried out a pair-wise feeding experiment where mice bearing Eμ-Myc tumors had either open access to food or restricted caloric intake equivalent to that ingested by Tsc2$^{+/-}$Eμ-Myc tumor-bearing mice (Fig. 2B). In this experiment, Eμ-Myc tumor-bearing mice in the pair-wise feeding cohort gained weight for 6 days, then when tumors were palpable (day 0), began losing weight albeit at a rate slower than Tsc2$^{+/-}$Eμ-Myc tumor-bearing mice. This contrasted to mice bearing Tsc2$^{+/-}$Eμ-Myc lymphomas who showed a dramatic weight loss upon appearance of palpable tumors (Fig. 2B). These results indicate that the loss of body weight observed in Tsc2$^{+/-}$Eμ-Myc tumor-bearing mice cannot simply be due to reduced caloric intake.

The earliest manifestation of deregulated metabolism (after day 7) in Tsc2$^{+/-}$Eμ-Myc tumor-bearing mice was a lowered RER, indicating a greater reliance on fat metabolism, even during the active nocturnal period (Fig. 2C). Given the low fat content of mouse chow this strongly suggests that reserve fuels in fat pads were being recruited (Fig. 2C). After day 12, the RER started climbing again suggesting that given the poor general condition and feeding of the animals at that time, amino acids from proteins (i.e., muscle and other organs) became a principal source of fuel. Tsc2$^{+/-}$Eμ-Myc tumor-bearing mice also showed a pronounced decrease in oxygen consumption, CO_2, and heat production, upon onset of palpable tumors, consistent with their inability to maintain a normal level of energy metabolism (Supplementary Fig. S4). This was also accompanied by a loss of the normal circadian variations in the level of metabolism in Tsc2$^{+/-}$Eμ-Myc tumor-bearing mice.

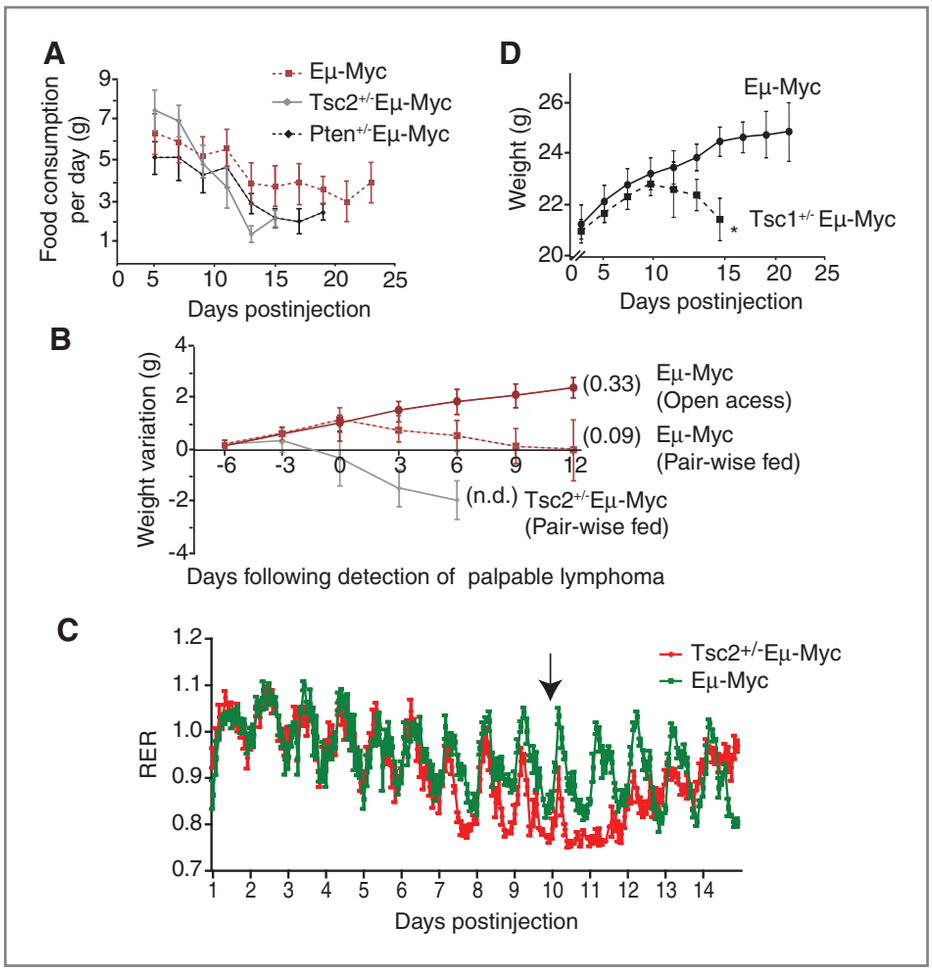

Figure 2. The anorexic component of ACS is recapitulated in mice bearing Tsc2$^{+/-}$Eμ-Myc tumors. A, food consumption of C57BL/6 mice bearing tumors of the indicated genotypes monitored every second day. B, pair-wise feeding of Eμ-Myc and Tsc2$^{+/-}$Eμ-Myc mice. Weight variation refers to the difference in weight of mice relative to day 3 following tumor cell injection (day −6 on graph). In parenthesis is the average weight of the epididymal fat pads at the end of the experiment; n.d., not detected. Values are mean ± SEM; $n = 5$ mice. C, alterations in RERs in mice bearing Tsc2$^{+/-}$Eμ-Myc or Eμ-myc tumors. The downward arrow indicates when palpable tumors were first detected. Values represent the mean ± SEM; $n = 4$ mice in each group. D, changes in body weight of C57BL/6 mice harboring tumors of the indicated genotypes. Values are mean ± SEM; $n = 5$ mice. *, indicates termination of experiment due to progression to endpoint.

Because TSC2 interacts with TSC1 to form a complex that inhibits mTOR signaling, we also evaluated whether Tsc1$^{+/-}$Eμ-Myc tumors would also yield an ACS phenotype. Tsc1$^{+/-}$Eμ-Myc tumor-bearing mice showed reduced survival rates compared with Eμ-Myc tumor-bearing animals (data not shown) and this was associated with a significant reduction in body weight (Fig. 2D) and loss of epididymal fat pads (data not shown). As documented for Tsc2$^{+/-}$Eμ-Myc tumor-bearing mice, Tsc1$^{+/-}$Eμ-Myc tumor-bearing mice had reduced appetite (Supplementary Fig. S5A). Tsc1$^{+/-}$Eμ-Myc tumors showed increased signaling flux through mTOR, as evidenced by increased phosphorylation of 4E-BP and rpS6 (Supplementary Fig. S5B). Taken together, these results indicate that mice bearing Eμ-Myc lymphomas with increased signaling flux through the Akt-mTOR axis, due to loss of Pten, Tsc1, or Tsc2 exhibit many features of ACS that are present in the human condition.

IL-10 is elevated in mice bearing Tsc2$^{+/-}$Eμ-Myc cells and is translationally regulated by mTOR

Another signature of the ACS phenotype in humans is what has been described as a "cytokine storm," the undesired production of cytokines that lead to a general systemic inflammatory response (1). To gain insight into the mechanism(s) driving ACS in Tsc2$^{+/-}$Eμ-Myc tumor-bearing mice, we quantitated serum levels of cytokines and known markers of cachexia in Tsc2$^{+/-}$Eμ-Myc and Eμ-Myc tumor-bearing mice (Table 1). The results indicate an impressive deregulation of cytokines and serum factors. We did not observe increases in the levels of the "classical" cachexia mediators and markers (e.g., IL-6, TNF-α, IFN-γ, and IL-1) in this model (21) but rather noted reduced levels of leptin and NPY and increased IL-10 and IL-12(p40) levels (1, 22). Similar changes in the profile of leptin and IL-10 were observed in skeletal muscle tissue from Tsc2$^{+/-}$Eμ-Myc tumor-bearing mice relative Eμ-Myc tumor-bearing mice or control C57BL/6 mice (Supplementary Fig. S6). Because of the implication of IL-10 in human ACS (see Discussion), we characterized regulation of IL-10 expression in Tsc2$^{+/-}$Eμ-Myc cells--focusing on translation as this is a major gene regulatory pathway usurped in Tsc2$^{+/-}$Eμ-Myc cells (14).

First, to uncouple drug-based effects on tumor cell maintenance from effects on procachexic factor production, we transduced the prosurvival gene encoding Mcl-1 into Tsc2$^{+/-}$Eμ-Myc cells (Fig. 3A and B) to generate drug resistant Tsc2$^{+/-}$Eμ-Myc/Mcl-1 cells (7). *Ex vivo*, both Tsc2$^{+/-}$Eμ-Myc and

Table 1. Cytokine profiling from C57BL/6, Eμ-Myc, and Tsc2$^{+/-}$Eμ-Myc tumor-bearing mice

Cytokine	C57BL/6[a]	Eμ-Myc[a]	Tsc2$^{+/-}$ Eμ-Myc[a]	*P* value[b] (Tsc2$^{+/-}$ Eμ-Myc vs. Eμ-Myc)
IL-1α	10.6 ± 5.1	9.2 ± 3.5	7.0 ± 2.7	
IL-1β	184.3 ± 52.5	239.1 ± 56.4	132.5 ± 52.7	<0.002
IL-2	18.0 ± 4.9	18.3 ± 4.1	12.4 ± 2.6	
IL-3	20.3 ± 3.6	26.1 ± 5.4	12.3 ± 6.6	<0.001
IL-5	14.8 ± 7.4	17.8 ± 4.2	8.5 ± 4.5	<0.001
IL-6	7.0 ± 3.6	11.9 ± 10.7	10.7 ± 5.3	
IL-9	317.8 ± 36.1	313.1 ± 59.8	218.5 ± 62.0	<0.003
IL-10	32.1 ± 8.1	61.7 ± 13.2	152.1 ± 36.4	<0.001
IL-12(p40)	191.7 ± 43.0	665.8 ± 178.2	1,273.4 ± 363.9	<0.001
IL-12(p70)	92.9 ± 18.9	62.4 ± 35.6	35.9 ± 25.1	
IL-13	776.8 ± 110.2	854.3 ± 192.1	489.4 ± 218.3	<0.004
IL-17	29.0 ± 10.2	31.2 ± 7.3	16.1 ± 8.5	<0.001
G-CSF	71.6 ± 13.8	322.0 ± 339.5	173.2 ± 231.3	
GM-CSF	63.0 ± 14.7	54.9 ± 19.0	43.3 ± 25.6	
IFN-γ	172.2 ± 29.4	247.2 ± 61.1	129.1 ± 55.1	<0.001
KC	64.6 ± 19.7	221.4 ± 157.7	156.2 ± 140.3	
MCP-1	378.4 ± 102.4	493.2 ± 175.8	241.6 ± 53.1	<0.004
MIP-1α	293.5 ± 43.6	230.7 ± 62.5	239.1 ± 54.5	
MIP-1β	46.9 ± 10.2	106.5 ± 32.3	51.3 ± 14.5	<0.001
RANTES	38.0 ± 3.0	29.6 ± 6.9	26.7 ± 7.4	
TNF-α	126.8 ± 34.9	153.8 ± 42.3	119.2 ± 36.6	<0.04
Leptin	85.3 ± 15.4	93.7 ± 33.2	5.3 ± 3.5	<0.001
Acetylated ghrelin	3.8 ± 0.5	4.0 ± 0.1	4.0 ± 0.2	
NPY	7.4 ± 2.6	9.93 ± 1.4	1.7 ± 0.6	<0.001
CRP, ng/mL	17 ± 0.3	22 ± 8	52 ± 16	<0.001
Glucose, μg/mL	100.6 ± 11.2	84.8 ± 7.4	55.6 ± 11.1	<0.001

[a]$n = 8$. Values expressed as average ±SD. Unless indicated otherwise, all values are expressed in pg/mL.
[b]Determined using the Student *t* test. If a value is not reported, then it was more than 0.05.

Tsc2$^{+/-}$Eμ-Myc/Mcl-1 cells produce higher levels of IL-10 than Eμ-Myc cells (Fig. 3C). IL-10 production in Tsc2$^{+/-}$Eμ-Myc/Mcl-1 cells was inhibited by rapamycin suggesting that it was under mTOR translational control (Fig. 3D). To more directly assess this, we isolated polysomes from rapamycin- and vehicle-treated Tsc2$^{+/-}$Eμ-Myc/Mcl-1 cells (Fig. 3E and Supplementary Fig. S7) and quantitated the distribution of IL-10 mRNA across the fractions. Rapamycin significantly reduced IL-10 mRNA translation, as assessed by a shift in the bulk IL-10 mRNA population from heavy to lighter polysomes (Fig 3F). This was an mRNA-selective effect as the distribution of β-actin mRNA did not change (Fig. 3G) upon exposure to rapamycin. These results show that IL-10 is a rapamycin-responsive mRNA whose translation is affected by signaling flux through the TSC1/2-mTOR pathway in Tsc2$^{+/-}$Eμ-Myc/Mcl-1 cells. Taken together, these results indicate that both muscle and Tsc2$^{+/-}$Eμ-Myc tumor cells are sources of increased IL-10 levels.

Inhibiting protein synthesis prolongs survival in ACS

We next rationalized that *in vivo* cytokine production could be inhibited by targeting mTOR (i.e., rapamycin) signaling or translation initiation (e.g., homoharringtonine), and that this might dampen the cytokine storm to ameliorate the severity of ACS in this model. To test this hypothesis, we first ensured that Tsc2$^{+/-}$Eμ-Myc/Mcl-1 cells were resistant to rapamycin and homoharringtonine *in vivo*. Indeed, animals bearing Tsc2$^{+/-}$Eμ-Myc/Mcl-1 cells do not respond to rapamycin or homoharringtonine compared with the tumor-free survival benefit afforded by these compounds in mice harboring Tsc2$^{+/-}$Eμ-Myc cells (Fig. 4A). Sufficient rapamycin and homoharringtonine was delivered *in vivo* to impair mTOR signaling protein synthesis in the tumor cell population, as respectively illustrated by decreased phosphorylation of 4E-BP1 and rpS6 (Supplementary Fig. S8A) and by the reduction of polysomes by homoharringtonine (Supplementary Fig. S8B) in Tsc2$^{+/-}$Eμ-Myc/Mcl-1 tumor cells. Tsc2$^{+/-}$Eμ-Myc/Mcl-1 tumor-bearing mice rapidly lost weight upon appearance of palpable tumors (Fig. 4B). Treatment of mice with rapamycin or homoharringtonine prevented this loss (Fig. 4B), improved appetite (Fig. 4C), and diminished the severity of fat loss (Fig. 4D), despite having little impact on the total tumor cell population (Fig. 4E). Both homoharringtonine and rapamycin significantly prolonged survival in mice bearing

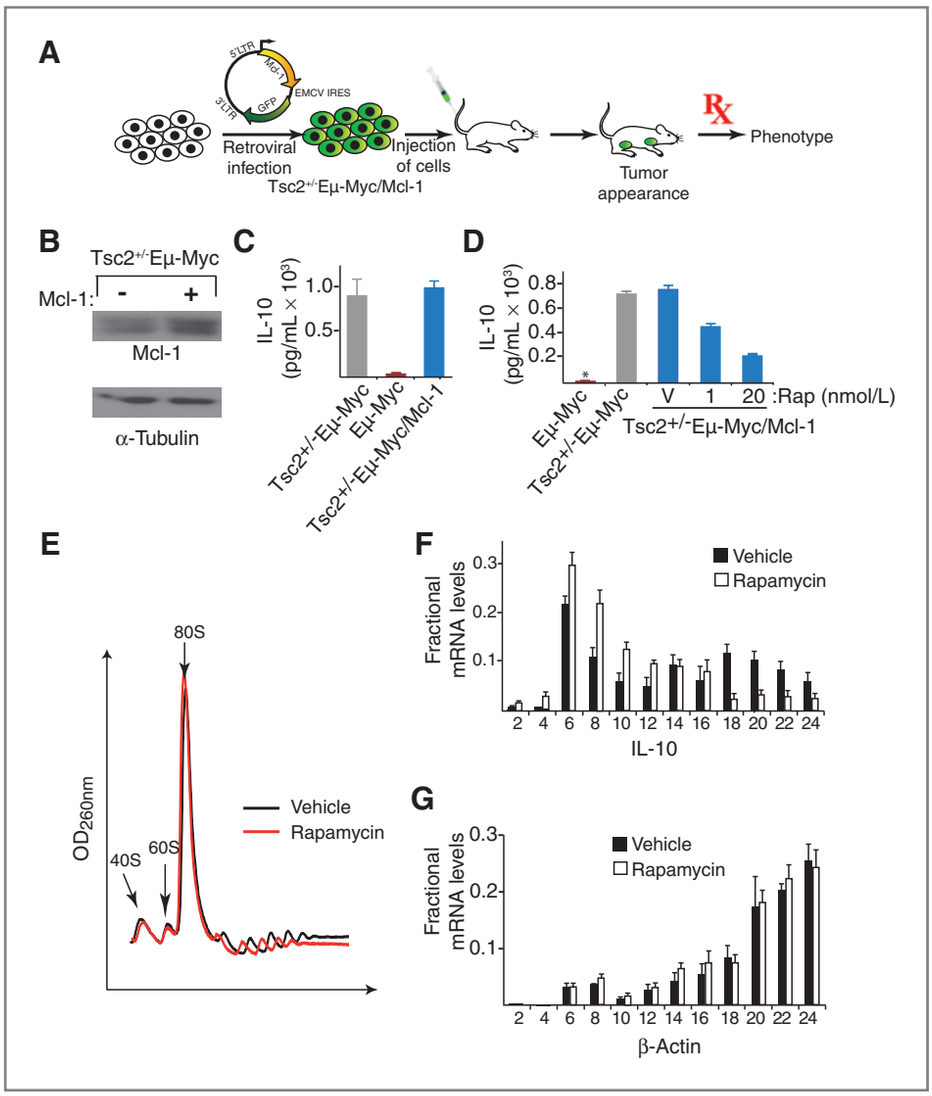

Figure 3. IL-10 is translationally regulated by mTOR. A, strategy used to generate rapamycin- and HTT-resistant Tsc2$^{+/-}$Eμ-Myc/Mcl-1 tumors. B, Western blotting of Mcl-1 levels in Tsc2$^{+/-}$Eμ-Myc and Tsc2$^{+/-}$Eμ-Myc/Mcl-1 cells. C, IL-10 levels obtained from supernatant of Tsc2$^{+/-}$Eμ-Myc, Tsc2$^{+/-}$Eμ-Myc/Mcl-1, or Eμ-Myc cells cultured *ex vivo*. Values are mean ± SEM; $n = 3$ samples. D, IL-10 production is inhibited by rapamycin. Tsc2$^{+/-}$Eμ-Myc/Mcl-1 cells were cultured *ex vivo* for 48 hours in the absence or presence of the indicated concentration of rapamycin and the growth medium probed for IL-10 by ELISA. Values are normalized to total protein content. Values are mean ± SEM; $n = 3$ samples. E, polysomes from vehicle- and rapamycin-treated Tsc2$^{+/-}$Eμ-Myc/Mcl-1 cells. F, inhibition of IL-10 mRNA translation by rapamycin. Tsc2$^{+/-}$Eμ-Myc/Mcl-1 cells were treated with 20 nmol/L rapamycin for 1 hour and polysomes fractionated on a sucrose gradient. Distribution of IL-10 across the polysome fractions of vehicle- and rapamycin-treated Tsc2$^{+/-}$Eμ-Myc/Mcl-1 cells was determined by qRT-PCR. G, distribution of β-actin mRNA across polysomes from vehicle- and rapamycin-treated Tsc2$^{+/-}$Eμ-Myc/Mcl-1 cells.

Tsc2$^{+/-}$Eμ-Myc/Mcl-1 tumors (Fig. 4F). As well, both rapamycin- and homoharringtonine-treated mice bearing Tsc2$^{+/-}$Eμ-Myc/Mcl-1 tumors showed significant improvements in the levels of several deregulated cytokines and markers (IL-10, CRP, and IL-12p40), leptin, NPY, and glucose (Supplementary Fig. S9). To determine whether these results could be explained by a general drug-mediated effect on muscle cell catabolism, we tested the ability of rapamycin to prevent IFN-γ/TNF-α–mediated muscle breakdown (23). We found that rapamycin was ineffective in preventing IFN-γ/TNF-α–induced weight loss and muscle degeneration in this model (Supplementary Fig. S10).

To extend these results and show they are not a peculiarity of the Eμ-Myc model, we tested rapamycin and homoharringtonine in another model of cancer cachexia—the C26 colon cancer model (Fig. 5A). This mouse model has been extensively studied and the cachexic phenotype is determined predominantly by high levels of the proinflammatory cytokine IL-6 (24–28), whose production is also under mTOR translational regulation (29). Treatment of C26 tumor-bearing mice with rapamycin, and to a lower extent homoharringtonine, also blunted several features of cachexia in this model, including loss of body weight (Fig. 5B), reduction in appetite (Fig. 5C), and the severity of fat loss (Fig. 5D), despite having little impact on total tumor weight (Fig. 5E). It is unclear why rapamycin is more effective than homoharringtonine in this model, but this may relate to mTOR contributing to the ACS phenotype in the C26 model through additional pathways that are translation independent.

Discussion

Herein, we characterize a novel model of ACS which displays many cardinal features of human ACS, including anorexia, increased expression of catabolic markers in muscle, reduced body weight, adipose tissue, muscle mass, total energy

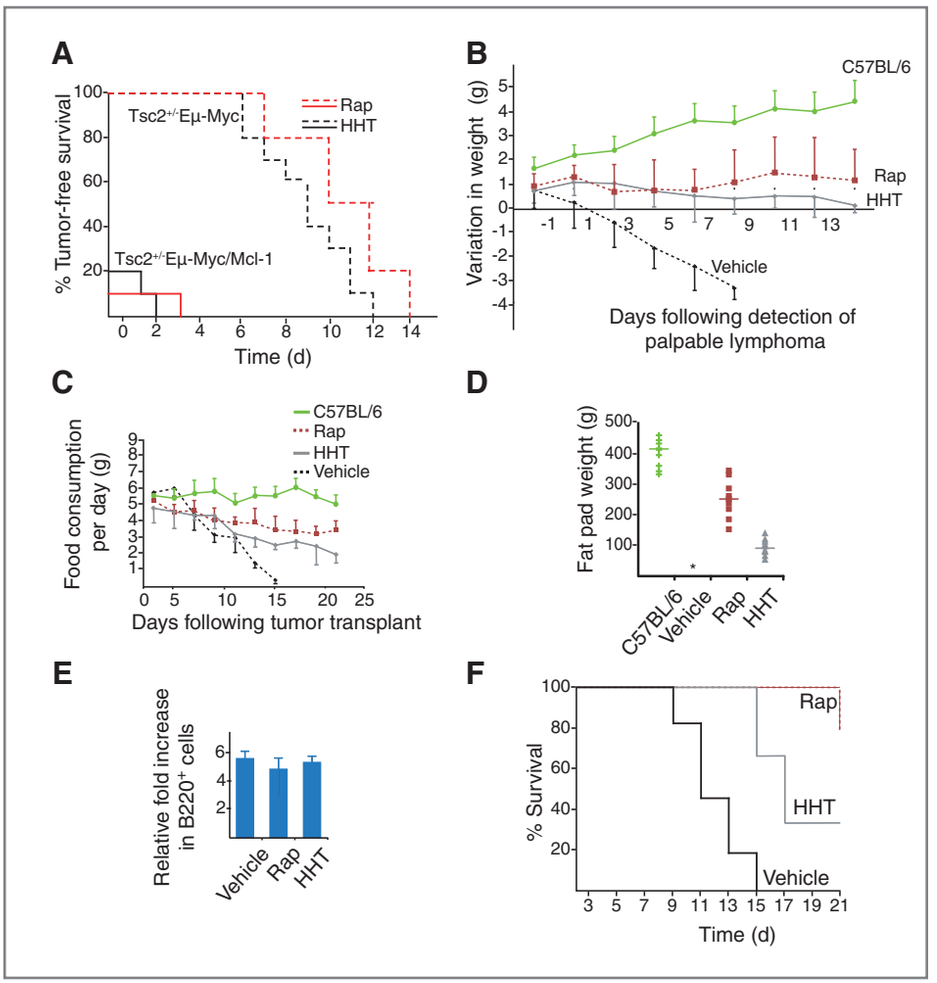

Figure 4. Inhibiting protein synthesis ameliorates ACS and prolongs survival in Tsc2$^{+/-}$Eμ-Myc/Mcl-1 tumor-bearing mice. A, Kaplan–Meier curve representing the time to relapse following treatment of Tsc2$^{+/-}$Eμ-Myc or Tsc2$^{+/-}$Eμ-Myc/Mcl-1 lymphoma-bearing mice with either rapamycin (Rap; 4 mg/kg) or homoharringtonine (HHT; 0.25 mg/kg). $n = 5$. B, variation in body weight of Tsc2$^{+/-}$Eμ-Myc/Mcl-1 lymphoma-bearing mice treated with rapamycin, homoharringtonine, or vehicle. Values are mean ± SEM; $n = 9$ mice. C, food consumption of mice from (B) monitored every second day. D, epididymal fat pad weights of wild-type or Tsc2$^{+/-}$Eμ-Myc/Mcl-1 lymphoma-bearing mice treated as indicated. Tissues were harvested at the end of the experiment in (B). Values are mean ± SEM; $n = 9$ mice. *, no fat pad remaining. E, fold increase of B220$^+$ cells in Tsc2$^{+/-}$Eμ-Myc/Mcl-1 lymphoma-bearing mice relative to non–tumor-bearing mice. Samples were taken 6 days following detection of palpable tumors. The number of B220$^+$ cells is set relative to the total cell population remaining after ACK lysis of red blood cells. Values are mean ± SEM; $n = 9$ mice. F, Kaplan–Meier curve detailing survival time following treatment of Tsc2$^{+/-}$Eμ-Myc/Mcl-1 lymphoma-bearing mice with rapamycin (4 mg/kg; $n = 9$), homoharringtonine (0.25 mg/kg; $n = 9$), or vehicle ($n = 9$). $P < 0.001$ for both rapamycin and homoharringtonine treated–mice compared with vehicle-treated mice.

expenditure, and survival. ACS is not a general feature of the Eμ-Myc model as mice bearing Eμ-Myc or Eμ-Myc/Bcl-2 lymphomas do not show signs of ACS (Fig. 1, Supplementary Figs. S2–S4). An important feature of our model is that the ACS phenotype presents itself at an early stage after tumor cell transplant before the tumor burden (lymphoma size, leukemic burden, and spleen size) is sufficiently large to impact on survival. This is exemplified by the fact that mice bearing Eμ-Myc tumor cells survive (Fig. 1A: 25 days) at least 2-fold beyond the time of first noticeable onset of ACS in Tsc2$^{+/-}$Eμ-Myc tumor-bearing mice (Fig. 1B: day 12). Hence our results cannot be attributed to an overwhelming tumor burden.

Several features of the model that we present encompass important components of human ACS and provide a powerful genetic system for future studies as follows. (i) Our model recapitulates tumor/host microenvironment by using immunocompetent animals. (ii) The Tsc2$^{+/-}$Eμ-Myc tumor-bearing model recapitulates deregulation of the appetite-controlling leptin/NPY axis present in human ACS (30, 31). Reduced leptin levels should increase NPY production to stimulate appetite, but the opposite is observed in the anorexigenic state in Tsc2$^{+/-}$Eμ-Myc tumor-bearing mice and is consistent with what has been reported for the human experience (reviewed in ref. 1). (iii) In Tsc2$^{+/-}$Eμ-Myc tumor-bearing mice, the onset of anorexia is reproducible and consistent–-a feature that is important when standardizing *in vivo* drug treatment protocols. (iv) In addition, our model easily lends itself to genetic manipulations as tumor cells can be expanded and

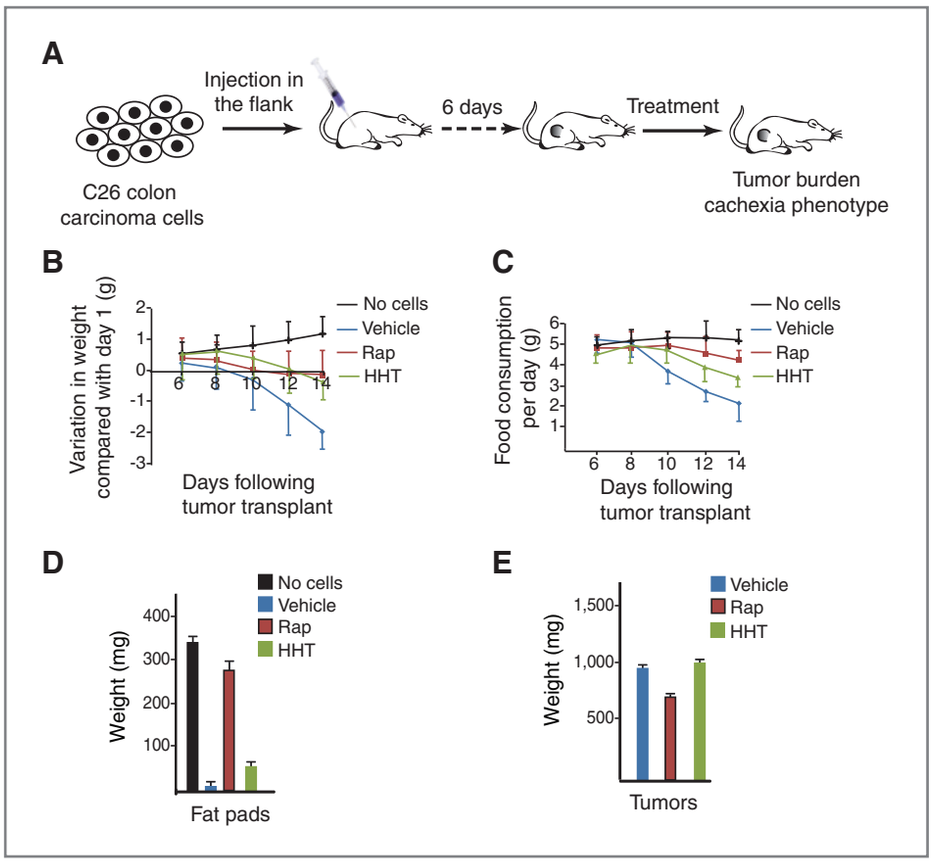

Figure 5. Rapamycin (Rap) and homoharringtonine (HHT) delay cachexia onset in the C26 colon cancer model. A, schematic outline of the C26 BALB/c transplantation and treatment protocol. B, body weight loss associated with vehicle-, rapamycin-, or homoharringtonine-treated C26 tumor-bearing mice. Values are mean ± SEM; $n = 6$ mice. C, food consumption associated in C26 tumor-bearing mice treated with the indicated compounds. Values are mean ± SEM; $n = 6$ mice. D, bar graph documenting adipose tissue in C26 tumor-bearing mice treated with the indicated compounds. Tissues were harvested at the end of experiment in (B). Values are mean ± SEM; $n = 6$ mice. E, bar graph documenting tumor burden in C26 tumor-bearing mice treated with the indicated compounds. Tissues were harvested at the end of experiment in (B). Values are mean ± SEM; $n = 6$ mice.

manipulated *ex vivo*, followed by transplantation experiments (Fig. 3A). (v) An increase in energy expenditure is also associated with human ACS (1). In some situations, this is manifested as an elevation in resting energy expenditure, whereas in others resting energy expenditure is increased whereas total energy expenditure is reduced, presumably because of reduced physical activity (1). Our model shows reduced total energy expenditure (Supplementary Fig. S4C). (vi) Muscle mass was also dramatically reduced in mice bearing $Tsc2^{+/-}$Eμ-Myc tumors and this coincided with activation of the ubiquitin system. Activation of this system in muscle has been observed in patients with cancer (32), suggesting that our model recapitulates this aspect of muscle wasting observed in human ACS. We also found activation of genes in the autophagy system which has recently been shown to be important in muscle wasting (20). To our knowledge there are no reports investigating the status of the autophagy system in human ACS, but it is known to be activated in human diaphragm muscle undergoing disuse atrophy (33).

We find that IL-10 and IL-12(p40) levels are significantly elevated in $Tsc2^{+/-}$Eμ-Myc tumor-bearing mice whereas levels of IL-6, IL-1, TNF-α, and IFN-γ remain unchanged or are decreased (Table 1). Hence, the classical markers of cachexia identified in other mouse models are not elevated in the $Tsc2^{+/-}$Eμ-Myc model. We characterized the mode of regulation of IL-10 in our model because of several reports of IL-10 dysregulation associated with human ACS. Shibata and colleagues (22) reported that IL-10 levels are elevated in patients with cachexic colorectal cancer compared with levels found in patients with colorectal cancer of all other stages. As well, patients with pancreatic cancer having high IL-10 levels show poorer overall survival than those with low IL-10 serum levels (34). Importantly, IL-10 promoter polymorphisms (35–37) are associated with elevated risk for cancer cachexia. How these polymorphisms predispose to cachexic onset is not known but one hypothesis could be that some lead to elevated IL-10 expression in tumors arising in said individuals. Consistent with IL-10 playing a role in the ACS phenotype of our model, we found that 11 of 13 different $Tsc2^{+/-}$Eμ-Myc cell lines were capable of generating the ACS phenotype described herein; all produced high levels of IL-10 in comparison with 2 lines that failed to generate an ACS phenotype and which showed baseline levels of IL-10 (data not shown). We note that IL-10 effects may be context dependent as in the C26 IL-6 driven cachexia model it has been shown to protect against cachexia (25, 38). Future experiments will be required to define which features of the ACS phenotype present in $Tsc2^{+/-}$Eμ-Myc tumor-bearing mice are due to elevated IL-10 levels.

We note also that the $Tsc2^{+/-}$Eμ-Myc model presents some differences with other cachexia models and the human condition. (i) Adipose tissue loss in human cachexia can vary significantly, ranging from considerable residual fat mass (39) to quite significant loss (40). In the $Tsc2^{+/-}$Eμ-Myc model, we clearly have an extreme effect of complete epididymal fat lost

at the terminal stage. (ii) As well, IL-6, a multifunctional cytokine, is strongly implicated in cachexia. Administration of IL-6 to mice is sufficient to recapitulate the muscle wasting and fat loss phenotype of ACS (41, 42), IL-6 blocking agents reduce the severity of muscle wasting in the C26 model (8, 24, 26, 27, 43, 44), and its overexpression is implicated in the pathogenesis of cachexia in several mouse models, including mice bearing the C26 cell line (5, 26, 45). One mechanism by which IL-6 has been implicated in this process is through activation of STAT3 signaling following binding to its receptor in muscle cells, leading to muscle-based production of acute phase proteins (28). It will be interesting to determine whether phospho-STAT3 levels are elevated in the $Tsc2^{+/-}$Eμ-Myc model. Along these lines, we note that IL-10 has also been shown to activate STAT3 in cardiomyocytes through an Akt-dependent mechanism (46). Were IL-6 and IL-10 to share a common effector target such as STAT3, this could suggest redundant roles for IL-6 and IL-10 in muscle wasting. (iii) Third, IL-6 expression in B cells may be regulated in a manner that precludes its overexpression. During development, IL-6 induces terminal differentiation and ultimately cell death of B cells (47). However, IL-6 can also participate in autocrine loops in some cancers to promote survival by signaling to the prosurvival protein, Mcl-1 (48). Because, Mcl-1 synergizes with Myc in the Eμ-Myc model to accelerate lymphomagenesis (49), expression of IL-6 may be tightly balanced in $Tsc2^{+/-}$/Eμ-Myc cells to sufficiently maintain antiapoptotic effects (through Mcl-1 upregulation) while avoiding cellular differentiation and death.

We found that in $Tsc2^{+/-}$Eμ-Myc cells IL-10 protein production was under mTOR translational control (Fig. 3D–F). Accordingly, inhibition of mTOR signaling or translation with rapamycin or homoharringtonine, respectively, alleviated the cachexic phenotype and correlated with reduced IL-10 mRNA translation. Rapamycin and homoharringtonine were also effective in the C26 mouse model where IL-6 is the major cachexic driver (Fig. 5). When considered together with the finding that IL-6 production is linked to mTOR activity (29), these results show that suppression of cytokine production by targeting translation may ameliorate the cachexic phenotype in some settings (Figs. 4 and 5). More extensive experiments will be required to determine whether rapamycin or homoharringtonine are exerting their effects by curtailing protein synthesis in $Tsc2^{+/-}$Eμ-Myc/Mcl-1 tumor cells, on host targets, or a combination of both.

Another strategy to prevent, and even reverse the effects of cachexia, has recently been described and involves inhibiting ActRIIB, a high affinity activin type 2 receptor involved in TGF-β signaling (50). Impressively, pharmacologic blockade of this pathway in muscles halts and reverses muscle wasting in cancer-induced cachexia (50). Currently, there is no approved effective treatment for muscle wasting in cachexia and targeting protein synthesis could complement muscle-directed therapies aimed at providing relief from ACS.

Disclosure of Potential Conflicts of Interest

No potential conflicts of interest were disclosed.

Acknowledgments

The authors thank Marilyn Carrier, Isabelle Harvey, and Nathalie Bédard for excellent technical assistance.

Grant Support

A. Agenor was supported by a CIHR Strategic Training Initiative in Chemical Biology and an FRSQ Fellowship. J. Pelletier is a holder of a James McGill Professor Award. S. Hekimi and D. Wang are supported by a grant from the Canadian Cancer Society Research Institute. This work was supported by grants from the Terry Fox Research Institute (to J. Pelletier, M.L. Tremblay, I.E. Gallouzi, and S.S. Wing), Canadian Institutes of Health Research (CIHR MOP-106530; to J. Pelletier), and a Canadian Cancer Society grant (NCIC 018125; to I.E. Gallouzi). J.R. Mills was supported by a CIHR Strategic Training Initiative in Chemical Biology and a Cole Foundation Fellowship. S. Hekimi is Robert Archibald & Catherine Louise Campbell Chair in Developmental Biology.

The costs of publication of this article were defrayed in part by the payment of page charges. This article must therefore be hereby marked *advertisement* in accordance with 18 U.S.C. Section 1734 solely to indicate this fact.

Received August 15, 2011; revised November 8, 2011; accepted November 28, 2011; published OnlineFirst December 12, 2011.

References

1. Tisdale MJ. Mechanisms of cancer cachexia. Physiol Rev 2009;89:381–410.
2. DeWys WD. Diet and cancer prevention: an overview. Semin Oncol 1983;10:255–6.
3. Kuroda K, Horiguchi Y, Nakashima J, Kikuchi E, Kanao K, Miyajima A, et al. Prevention of cancer cachexia by a novel nuclear factor {kappa}B inhibitor in prostate cancer. Clin Cancer Res 2005;11:5590–4.
4. Muscaritoli M, Bossola M, Aversa Z, Bellantone R, Rossi Fanelli F. Prevention and treatment of cancer cachexia: new insights into an old problem. Eur J Cancer 2006;42:31–41.
5. Bibby MC, Double JA, Ali SA, Fearon KC, Brennan RA, Tisdale MJ. Characterization of a transplantable adenocarcinoma of the mouse colon producing cachexia in recipient animals. J Natl Cancer Inst 1987;78:539–46.
6. Beck SA, Tisdale MJ. Production of lipolytic and proteolytic factors by a murine tumor-producing cachexia in the host. Cancer Res 1987;47:5919–23.
7. Matsumoto T, Fujimoto-Ouchi K, Tamura S, Tanaka Y, Ishitsuka H. Tumour inoculation site-dependent induction of cachexia in mice bearing colon 26 carcinoma. Br J Cancer 1999;79:764–9.
8. Davis TW, Zweifel BS, O'Neal JM, Heuvelman DM, Abegg AL, Hendrich TO, et al. Inhibition of cyclooxygenase-2 by celecoxib reverses tumor-induced wasting. J Pharmacol Exp Ther 2004;308:929–34.
9. Altomare DA, Testa JR. Perturbations of the AKT signaling pathway in human cancer. Oncogene 2005;24:7455–64.
10. Sonenberg N, Hinnebusch AG. Regulation of translation initiation in eukaryotes: mechanisms and biological targets. Cell 2009;136:731–45.
11. Wendel HG, De Stanchina E, Fridman JS, Malina A, Ray S, Kogan S, et al. Survival signalling by Akt and eIF4E in oncogenesis and cancer therapy. Nature 2004;428:332–7.
12. Bordeleau ME, Robert F, Gerard B, Lindqvist L, Chen SM, Wendel HG, et al. Therapeutic suppression of translation initiation modulates

chemosensitivity in a mouse lymphoma model. J Clin Invest 2008;118:2651–60.
13. Adams JM, Harris AW, Pinkert CA, Corcoran LM, Alexander WS, Cory S, et al. The c-myc oncogene driven by immunoglobulin enhancers induces lymphoid malignancy in transgenic mice. Nature 1985;318:533–8.
14. Mills JR, Hippo Y, Robert F, Chen SM, Malina A, Lin CJ, et al. mTORC1 promotes survival through translational control of Mcl-1. Proc Natl Acad Sci U S A 2008;105:10853–8.
15. United Kingdom Co-ordinating Committee on Cancer Research (UKCCCR). Guidelines for the welfare of animals in experimental neoplasia (second edition). Br J Cancer 1998;77:1–10.
16. McLean JA, Tobin G. Animal and human calorimetry. Cambridge, UK: Cambridge University Press; 1987.
17. Bodine SC, Latres E, Baumhueter S, Lai VK, Nunez L, Clarke BA, et al. Identification of ubiquitin ligases required for skeletal muscle atrophy. Science 2001;294:1704–8.
18. Gomes MD, Lecker SH, Jagoe RT, Navon A, Goldberg AL. Atrogin-1, a muscle-specific F-box protein highly expressed during muscle atrophy. Proc Natl Acad Sci U S A 2001;98:14440–5.
19. Combaret L, Adegoke OA, Bedard N, Baracos V, Attaix D, Wing SS. USP19 is a ubiquitin-specific protease regulated in rat skeletal muscle during catabolic states. Am J Physiol Endocrinol Metab 2005;288:E693–700.
20. Mammucari C, Milan G, Romanello V, Masiero E, Rudolf R, Del Piccolo P, et al. FoxO3 controls autophagy in skeletal muscle *in vivo*. Cell Metab 2007;6:458–71.
21. Argiles JM, Busquets S, Lopez-Soriano FJ. Anti-inflammatory therapies in cancer cachexia. Eur J Pharmacol 2011;668 Suppl 1:S81–6.
22. Shibata M, Nezu T, Takekawa M, Takizawa H, Ando K, Miyake H, et al. Serum levels of interleukin-10 and interleukin-12 in patients with colorectal cancer. Ann N Y Acad Sci 1996;795:410–2.
23. Llovera M, Garcia-Martinez C, Agell N, Lopez-Soriano FJ, Argiles JM. TNF can directly induce the expression of ubiquitin-dependent proteolytic system in rat soleus muscles. Biochem Biophys Res Commun 1997;230:238–41.
24. Strassmann G, Fong M, Freter CE, Windsor S, D'Alessandro F, Nordan RP. Suramin interferes with interleukin-6 receptor binding *in vitro* and inhibits colon-26-mediated experimental cancer cachexia *in vivo*. J Clin Invest 1993;92:2152–9.
25. Mori K, Fujimoto-Ouchi K, Ishikawa T, Sekiguchi F, Ishitsuka H, Tanaka Y. Murine interleukin-12 prevents the development of cancer cachexia in a murine model. Int J Cancer 1996;67:849–55.
26. Strassmann G, Fong M, Kenney JS, Jacob CO. Evidence for the involvement of interleukin 6 in experimental cancer cachexia. J Clin Invest 1992;89:1681–4.
27. Strassmann G, Jacob CO, Fong M, Bertolini DR. Mechanisms of paraneoplastic syndromes of colon-26: involvement of interleukin 6 in hypercalcemia. Cytokine 1993;5:463–8.
28. Bonetto A, Aydogdu T, Kunzevitzky N, Guttridge DC, Khuri S, Koniaris LG, et al. STAT3 activation in skeletal muscle links muscle wasting and the acute phase response in cancer cachexia. PLoS One 2011;6:e22538.
29. Lehle K, Birnbaum DE, Preuner JG. Predominant inhibition of interleukin-6 synthesis in patient-specific endothelial cells by mTOR inhibitors below a concentration range where cell proliferation is affected and mitotic arrest takes place. Transplant Proc 2005;37:159–61.
30. Simons JP, Schols AM, Campfield LA, Wouters EF, Saris WH. Plasma concentration of total leptin and human lung-cancer-associated cachexia. Clin Sci (Lond) 1997;93:273–7.
31. Jatoi A, Loprinzi CL, Sloan JA, Klee GG, Windschitl HE. Neuropeptide Y, leptin, and cholecystokinin 8 in patients with advanced cancer and anorexia: a North Central Cancer Treatment Group exploratory investigation. Cancer 2001;92:629–33.
32. Williams A, Sun X, Fischer JE, Hasselgren PO. The expression of genes in the ubiquitin-proteasome proteolytic pathway is increased in skeletal muscle from patients with cancer. Surgery 1999;126:744–9; discussion 749–50.
33. Hussain SN, Mofarrahi M, Sigala I, Kim HC, Vassilakopoulos T, Maltais F, et al. Mechanical ventilation-induced diaphragm disuse in humans triggers autophagy. Am J Respir Crit Care Med 2010;182:1377–86.
34. Ebrahimi B, Tucker SL, Li D, Abbruzzese JL, Kurzrock R. Cytokines in pancreatic carcinoma: correlation with phenotypic characteristics and prognosis. Cancer 2004;101:2727–36.
35. Deans DA, Tan BH, Ross JA, Rose-Zerilli M, Wigmore SJ, Howell WM, et al. Cancer cachexia is associated with the IL10-1082 gene promoter polymorphism in patients with gastroesophageal malignancy. Am J Clin Nutr 2009;89:1164–72.
36. Sun F, Sun Y, Yu Z, Zhang D, Zhang J, Song B, et al. Interleukin-10 gene polymorphisms influence susceptibility to cachexia in patients with low-third gastric cancer in a Chinese population. Mol Diagn Ther 2010;14:95–100.
37. Sun F, Sun Y, Zhang D, Zhang J, Song B, Zheng H. Association of interleukin-10 gene polymorphism with cachexia in Chinese patients with gastric cancer. Ann Clin Lab Sci 2010;40:149–55.
38. Fujiki F, Mukaida N, Hirose K, Ishida H, Harada A, Ohno S, et al. Prevention of adenocarcinoma colon 26-induced cachexia by interleukin 10 gene transfer. Cancer Res 1997;57:94–9.
39. Lieffers JR, Mourtzakis M, Hall KD, McCargar LJ, Prado CM, Baracos VE. A viscerally driven cachexia syndrome in patients with advanced colorectal cancer: contributions of organ and tumor mass to whole-body energy demands. Am J Clin Nutr 2009;89:1173–9.
40. Fearon KC. The Sir David Cuthbertson Medal Lecture. 1991. The mechanisms and treatment of weight loss in cancer. Proc Nutr Soc 1992;51:251–65.
41. Ohe Y, Podack ER, Olsen KJ, Miyahara Y, Miura K, Saito H, et al. Interleukin-6 cDNA transfected Lewis lung carcinoma cells show unaltered net tumour growth rate but cause weight loss and shortened survival in syngeneic mice. Br J Cancer 1993;67:939–44.
42. Black K, Garrett IR, Mundy GR. Chinese hamster ovarian cells transfected with the murine interleukin-6 gene cause hypercalcemia as well as cachexia, leukocytosis and thrombocytosis in tumor-bearing nude mice. Endocrinology 1991;128:2657–9.
43. Tamura S, Ouchi KF, Mori K, Endo M, Matsumoto T, Eda H, et al. Involvement of human interleukin 6 in experimental cachexia induced by a human uterine cervical carcinoma xenograft. Clin Cancer Res 1995;1:1353–8.
44. Fujita J, Tsujinaka T, Ebisui C, Yano M, Shiozaki H, Katsume A, et al. Role of interleukin-6 in skeletal muscle protein breakdown and cathepsin activity *in vivo*. Eur Surg Res 1996;28:361–6.
45. Strassmann G, Jacob CO, Evans R, Beall D, Fong M. Mechanisms of experimental cancer cachexia. Interaction between mononuclear phagocytes and colon-26 carcinoma and its relevance to IL-6-mediated cancer cachexia. J Immunol 1992;148:3674–8.
46. Dhingra S, Bagchi AK, Ludke AL, Sharma AK, Singal PK. Akt Regulates IL-10 Mediated Suppression of TNFalpha-Induced Cardiomyocyte Apoptosis by Upregulating Stat3 Phosphorylation. PLoS One 2011;6:e25009.
47. Cheung WC, Van Ness B. Distinct IL-6 signal transduction leads to growth arrest and death in B cells or growth promotion and cell survival in myeloma cells. Leukemia 2002;16:1182–8.
48. Cavarretta IT, Neuwirt H, Untergasser G, Moser PL, Zaki MH, Steiner H, et al. The antiapoptotic effect of IL-6 autocrine loop in a cellular model of advanced prostate cancer is mediated by Mcl-1. Oncogene 2007;26:2822–32.
49. Wendel HG, Silva RL, Malina A, Mills JR, Zhu H, Ueda T, et al. Dissecting eIF4E action in tumorigenesis. Genes Dev 2007;21:3232–7.
50. Zhou X, Wang JL, Lu J, Song Y, Kwak KS, Jiao Q, et al. Reversal of cancer cachexia and muscle wasting by ActRIIB antagonism leads to prolonged survival. Cell 2010;142:531–43.